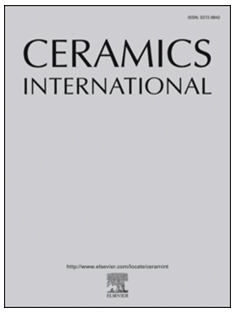

Multifunctional behavior of acceptor-cation substitution at higher doping concentration in PZT ceramics

Nitu Kumari, Shagun Monga, Mohd Arif, Neeraj Sharma, Amit Sanger, Arun Singh, Paula M. Vilarinho, Vinay Gupta, K. Sreenivas, Ram S. Katiyar, James F. Scott

PII: S0272-8842(19)30671-6

DOI: https://doi.org/10.1016/j.ceramint.2019.03.138

Reference: CERI 21077

To appear in: *Ceramics International*

Received Date: 19 December 2018

Revised Date: 14 March 2019

Accepted Date: 19 March 2019

Please cite this article as: N. Kumari, S. Monga, M. Arif, N. Sharma, A. Sanger, A. Singh, P.M. Vilarinho, V. Gupta, K. Sreenivas, R.S. Katiyar, J.F. Scott, Multifunctional behavior of acceptor-cation substitution at higher doping concentration in PZT ceramics, *Ceramics International* (2019), doi: https://doi.org/10.1016/j.ceramint.2019.03.138.

Multifunctional Behavior of acceptor-cation substitution at higher doping concentration in PZT ceramics

Nitu Kumari,[1] Shagun Monga,[1] Mohd. Arif, [1] Neeraj Sharma, [1] Amit Sanger, [3] Arun Singh,[1,6*] Paula. M. Vilarinho,[4] Vinay Gupta,[5] K. Sreenivas,[5] Ram S. Katiyar[6], James F. Scott[7]

[1]*Advanced Electronic and Nano-Materials Laboratory, Department of Physics, Jamia Millia Islamia University, New Delhi- 110025, India*
[2]*Department of Physics, TMB University, Bhagalpur, 812007 India*
[3]*Department of Materials Science and Engineering, Ulsan National Institute of Science and Technology, Ulsan 44919, Republic of Korea*
[4]*Department of Ceramics and Glass Engineering, University of Aveiro, 3810-193 Aveiro, Portugal*
[5]*Electronic Materials and Device Laboratory, Department of Physics and Astrophysics, University of Delhi, Delhi-110 007, India*
[6]*SPECLAB, Department of Physics, University of Puerto Rico, San Juan 00931, Puerto Rico, USA.*
[7]*Department of Physics, University of St Andrews, St Andrews-KY16 9SS, UK*

[a)] ***Corresponding author***
Dr. Arun Singh,
Assistant Professor
Department of Physics, Faculty of Natural Science
Jamia Millia Islamia (a Central University),
New Delhi, India, 110025
Email:***arunsingh07@gmail.com,***
Tel.: +91-26984631; +91-9891223302

Abstract

The Fe-doped PZT, Pb $(Zr, Ti)_{1-x}Fe_xO_3$, ceramics have gathered plenty of attention because of the interplay of ferroelectric and ferromagnetic properties. In the present study, we report the properties of $Pb(Zr_{0.52}Ti_{0.48})_{1-x}Fe_xO_3$, x = 0, 0.05, 0.10, 0.15 and 0.20, prepared by conventional solid state reaction route with varying Fe^{3+} doping concentrations. Study of X- ray diffraction patterns confirmed the tetragonal crystal structure with reduction in tetragonality and unit cell size with doping. It also showed formation of secondary magneto-plumbite phase at higher doping concentrations. The SEM micrographs exhibited decrease in grain size with increase in doping concentration (for x > 0.05). The increase in oxygen vacancies and the formation of secondary magneto-plumbite phase and Fe^{3+}–VO^{2-}–Fe^{3+} defect dipole complexes introduced with the acceptor (Fe^{3+}) doping, caused clamping of the domain walls and hence reduced the room temperature dielectric constant as the doping concentration was increased. The coexistence of electrical polarization and magnetic moment at room temperature in all PFZT compositions confirmed the multiferroic characteristic in the ceramic samples. Electric polarization (P_r) and coercive fields (E_c) decreased with increase in Fe^{3+} concentration in PFZT sample. However, magnetization (M) and magnetic coercive fields (E_c) increased with the increasing Fe^{3+} concentration due to the dominant effect of F-center exchange mechanism in Fe^{3+}–VO^{2-}–Fe^{3+} and formation of ferromagnetic secondary magneto-plumbite phase.

Key Words: Ferroelectric, Multiferroic, Ceramics, PFZT, XRD, SEM, Dielectric, Magnetization

1. Introduction

Ceramics encompass an extensive number of various materials. They are generally defined as inorganic non-metallic compounds, which includes a wide range of contemporary highly functional and cutting-edge materials. Such materials manifest a comprehensive range of valuable properties such as thermal resistance, ultimate rigidity/stiffness, chemical stability, and lasting strengths. Some of these materials, known as advanced ceramics, are engineered accurately to attain specific properties and are known to surpass the severities of industrial and technological applications. With the ongoing investigation of new materials, their properties and applications, the ceramics industry can be said to be in its blooming stage with its full potential still in evaluation. Consequently, several functional metal oxides have also been studied [1-5]. Lead Zirconate - Lead Titanate (PZT) solid solution is the most renowned ferroelectric material being employed for diverse purposes such as high energy-storage devices, ultrasonic detectors, hydrophones, transducers, infra-red detectors, electro optic devices, and nonvolatile memories (FERAM) [6–14]. The ferroelectric PZT crystallizes in ABO_3 perovskite structure, Fig. 1, with Pb^{2+} (Ionic radii = 1.49Å) occupying the A site and both Zr^{4+} (Ionic radii = 0.72Å) and Ti^{4+} (Ionic radii = 0.605 Å) occupying the B site. The properties of the PZT material such as electrical, piezoelectric, ferroelectric, etc. can be altered significantly by introduction of foreign ions at A and/or B-sites of the perovskite. The incorporation of dopants at A and B sites is related more to the size of the doping ion than to its properties. Therefore, the A-site occupied by Pb^{2+} ($r_{Pb^{2+}}$ = 1.49 Å) may be replaced by ions of similar ionic radii such as by K^+ (r_{K^+} = 1.64), Na^+ (r_{Na^+} = 1.39 Å) which act as acceptors or La^{3+} ($r_{La^{3+}}$ = 1.36 Å), Bi^{3+} ($r_{Bi^{3+}}$ = 1.17 Å), Nd^{3+} ($r_{Nd^{3+}}$ = 1.27 Å) which act as donor. Likewise, the Ti^{4+} and Zr^{4+} ions occupying the B-sites may be substituted by acceptors Al^{3+} ($r_{Al^{3+}}$ = 0.535 Å), Mn^{3+} ($r_{Mn^{3+}}$ = 0.645 Å) or donor Nb^{5+}

($r_{Nb^{5+}}$ = 0.78 Å), Sb^{5+} ($r_{Sb^{5+}}$ = 0.60 Å) owing to their probable ionic radii [15-19]. The addition of Fe^{3+} to PZT ceramics is of particular interest as it shows varied effects depending on the content of doping or solubility limit in PZT. According to the literature review introduction of Fe^{3+} ($r_{Fe^{3+}}$ = 0.645 Å) substitutes the B-site cations and generates charge compensating oxygen vacancies (eq.1):

$$Fe_2O_3 + 2Ti + O_O \rightarrow 2Fe_{Ti}{}' + V_{\ddot{o}} + 2TiO_2 \qquad (1)$$

Also, the Fe-doping forms defect dipole complexes, Fe^{3+}–VO^{2-}–Fe^{3+}, associated with the generated oxygen vacancies which tends to align with the bulk polarization and is stable at the domain walls. The result is hard ferroelectric effects i.e. reduced dielectric constant, piezoelectric coefficients, remnant polarization and increased coercive field. According to the reported literature, Fe^{3+} ions have a limited solubility in PZT i.e. below 1%. Addition of Fe^{3+} above this solubility limit leads to formation of secondary phases at multigrain junctions or along grain boundaries, which has not been explored much [2, 20- 24].

Apart from modification of the materials for tailoring of its properties, certain dopants may introduce concurrence of two or more properties creating possibilities for new applications. One class of such multifunctional materials is called multiferroics which exhibits both ferroelectric and ferromagnetic properties. The association among unlike properties permits for an extra degree of freedom while designing a device, hence the multiferroic materials are both physically fascinating and technologically significant [20, 25–31]. However, the simultaneous existence of both spontaneous magnetization and electric polarization at room temperature has been discovered in very few materials.

Consequently, this work reports an effort to generate ferromagnetism along with inherent ferroelectric properties in PZT ceramics by doping it with Fe^{3+} ions way above their solubility

limit (Fe = 0, 5, 10, 15, and 20 at%). The incorporation site (A or B-site) for the added Fe^{3+} was determined using the Goldschmidt or tolerance factor, eq.2 [23, 32]:

$$t = \frac{r_A + r_O}{\sqrt{2}(r_B + r_O)} \qquad (2)$$

Here, r_A, r_B and r_O represents the ionic radii of the occupants of A-site, B-site and O-site of ABO_3 perovskite, respectively. The tolerance factors for the A and B sites of the Fe-doped PZT ceramics with Fe^{3+} = 0.645 Å, was obtained to be 0.70 and 0.99, respectively. These values indicate that Fe^{3+} would replace the B-site cations while acting as an acceptor as higher values of tolerance factor leads to a perovskite structure with higher stability.

Our work here presents a systematic investigation of effects of Fe-doping on the structural, electrical and multiferroic properties of PZT ceramics prepared via the conventional solid-state reaction method with Fe-concentrations of 0, 5, 10, 15 and 20 at%. Great attention has been invested in the investigation of properties of Fe-doped PZT ceramics at lower Fe-doping concentrations. A comparative report of different properties reported for different doping concentration of Fe in PZT ceramics in earlier literatures can be seen in Table. 1. There is hardly any work reporting the effects of excessive Fe-doping in PZT ceramics. Thus, we have focused our investigation on the properties of Fe-doped PZT ceramics at higher doping concentrations which have not been reported yet.

2. Experimental procedure

Fe-doped PZT (PZTF) ceramics near morphotropic phase boundary composition, $Pb(Zr_{0.52}Ti_{0.48})_{1-x}Fe_xO_3$ with x = 0.00 to 0.20, were synthesized via the conventional technique of solid-state reaction shown in the flow chart given in Fig. 2 [33-36]. Lead oxide (PbO), zirconium oxide (ZrO_2), titanium oxide (TiO_2) and iron (III) oxide (Fe_2O_3) were used as the raw materials.

These oxide compounds were dried in oven to remove moisture and then weighed according to the required stoichiometry and doping content. The weighed oxides were mixed together in different batches (PZT-F0, PZT-F5, PZT-F10, PZT-F15 and PZT-F20 for x = 0, 5, 10, 15 and 20 at.%). The respective mixed oxides batches were grinded thoroughly for 4 hours in alcohol medium using agate mortar and pestle. The homogenized powdered mixtures were then calcined at 800°C for 5 hours. After calcination the powders were again grinded and a little amount of polyvinyl alcohol (PVA) was blended in it to reduce the brittleness and increase the compactness required in a ceramic material. These powders were hydraulic-pressed into green pellets of 12 mm diameter and 1.5 mm thickness using a pressure of 6 ton/cm^2 and then sintered in the presence of oxygen in a programmable furnace at 1200°C for 2 hours with a heating rate of 5°C/min. A closed crucible dusted with calcined $PbZrTiO_3$ powder was used to produce increased partial pressure of lead oxide within the crucible and hence decrease the rate of loss of lead oxide during sintering. These ceramic samples were investigated for their structural properties using x-ray diffraction (XRD), scanning electron microscopy (SEM) and Raman spectroscopy. The XRD studies were performed at room temperature using the Bruker D8 X-ray diffractometer in the range 2θ = 20° - 80°, step size 0.02°, examining rate 1°/min and Cu k_α radiation. To comprehend the size and distribution of grains in the Fe-doped PZT ceramic pellets SEM micrographs were obtained using Carl Zeiss Evo40. The Raman spectra of the samples were obtained in the wave number range of 400-1200 cm^{-1} with spectral resolution of 0.4 cm^{-1}. The Fe-doped PZT ceramic samples, in metal-insulator-metal configuration, were examined for their dielectric properties using Agilent 4284A precision LCR meter in the frequency range of 20 Hz to 1 MHz. The P-E hysteresis curves for the samples were recorded at room temperature using an automatic P-E loop tracer system. The ferromagnetic properties were investigated by

studying the B-H hysteresis curves for the ceramic samples recorded at room temperature using LAKE SHORE vibrating sample magnetometer.

3. Results and Discussion

3.1. Structural characterization

3.1.1. X – Ray Diffraction

Fig. 3 shows the XRD patterns for the PZTF (x = 0, 5, 10, 15, 20 at%), ceramic samples with many sharp peaks indicating formation of crystals with long-range periodic atomic order. All the Bragg's peaks in the XRD patterns for PZTF ceramic samples were indexed and Miller indices (hkl) were assigned to them in reference to the data reported by the Joint Committee on Powder Diffraction Standards (JCPDS) for $Pb(Zr_{0.52}Ti_{0.48})O_3$ in the File # 33-0784. The XRD patterns showed no deviation in the basic crystal symmetry and confirmed creation of single tetragonal phase with P4mm space group in Fe-doped PZT ceramic compositions, with appearance of secondary magneto-plumbite ($PbFe_{12}O_{19}$) phase on addition of Fe^{3+} in the PZT ceramic system [20,37]. Table. 2 and Fig. 4(a) shows the lattice parameters for the Fe-doped PZT ceramic compositions as calculated from the XRD data. The increase in content of Fe-doping slightly increased the value of lattice constant '*a*' while the lattice constant c was observed to decrease, which is likely to occur when a large ion such as Fe^{3+} (0.645 Å) substitutes a smaller ion like Ti^{4+} (0.605 Å). The subsequent reduction in the c/a ratio signifies repression of ferroelectric distortion [15, 38-40]. Fig. 4(b) shows the shifting of the XRD peaks to higher 2θ with increase in the Fe-doping concentration. The shift suggests a homogenous strain that can be attributed to the difference between Fe^{3+} and Ti^{4+} ionic radii. Fig. 4(c) represents the lattice strain calculated from the XRD data (Table. 2).

The crystallite size for PZTF ceramic compositions was calculated using the Debye-Scherrer equation (3) [41]:

$$D = 0.98\lambda/\beta \cos\theta \qquad (3)$$

Fig. 5(a) shows the variation of crystallite size values calculated from above equation. These values uncover the nano-crystalline character of the ceramic samples. Also, it shows a decrease in crystallite size with increase in Fe-doping concentration, a trend which have been reported by others also, inset of Fig. 5(a). The lattice parameters were used to calculate the unit cell size, Fig. 5(b), which also decreased with increase in Fe-doping. A similar trend has been reported by others also [15, 38, 42]. This is reflected in the observed shift in XRD peaks to higher 2θ, Fig. 4(b).

3.1.2. Grain Size

Fig. 6 shows the micrographs of sintered PFZT ceramics obtained using Scanning Electron Microscopy (SEM). The SEM images show polycrystalline grains spread all over the material's surface in non-homogeneous manner. The average grain size calculated from the micrographs of Fe-doped PZT ceramic samples is shown in Table. 2 and Fig. 7. The pure PZT ceramic sample contained grains with an average size of 0.41 µm. On introducing 5 at.% of Fe^{3+} in PZT the grain size decreased to 0.25 µm and it kept on decreasing on further addition of the dopant which suggest the restraining effect of Fe^{3+} ions on grain growth caused by their lower mobility due to the larger ionic radius and atomic weight in comparison to Ti^{4+} ions. Also, the grain boundary motion is restricted by the accumulation of Fe^{3+} and secondary magneto-plumbite phase at the grain boundary resulting in reduced grain growth [15,39,43]. This decrease in grain size with increase in doping concentration has also been reported in earlier literatures as can be seen in Table. 1 and inset of Fig. 7.

3.1.3. Raman spectroscopy study

Raman scattering is an efficient, non-destructive, sensitive, qualitative and subtle method for micro-structural studies and probing of local deviations from the average symmetry of a material such as those which arise from addition of foreign atom or change in composition. This technique has extensively been used for the investigation of phase structure of polycrystalline ferroelectric ceramics. In the ferroelectric PZT-based ceramics, this characterization technique has been implemented to investigate the phase co-existence, to study the MPB at low temperatures, to examine the different phase transition in a range of temperatures, to explore the structural effects of addition of dopants, and to address the effect of particle size on the Raman phonon modes and MPB [44-46].

The $3T_{1u} + T_{2u}$ Raman modes of cubic paraelectric phase transforms as $3A_1 + 4E + B_1$ irreducible representation for the P4mm tetragonal PZT. These are labelled as A_1(nTO), A_1(nLO), E(nTO), E(nLO) and B_1 + E, with the index n = 1, 2, 3 increasing with the frequency [39, 47-48]. Raman scattering was carried out in order to explore the effects of Fe-substitution on PZT crystal structure. Fig. 8(a) shows the Raman spectra for the Fe-doped PZT ceramic samples at room temperature (RT). The Raman modes were identified and labeled in reference to the previous reported works (Table. 3). It can be observed from the Fig. 8(a) that the doped ceramic samples have more or less similar spectra to that of pure PZT. Pure PZT and Fe-doped samples displayed chief peaks around 91, 125, 200, 263, 545, 702 cm^{-1} represented by E(1LO), A_1(1TO), E(2TO), B_1 + E, E(3TO), E(3LO) character and weaker modes around 70, 309 cm^{-1} with E(1TO), A_1(2TO) respectively.

In comparison to pure PZT the Raman spectra of Fe-doped PZT for Fe = 5, 10, 15 and 20 at% seems to be somewhat displaced to the higher wave numbers, Fig. 8(b), which is owed to the difference in the ionic radii and weights of Ti^{4+} and Fe^{3+}. This shift implies an increase in force

constant as the substitution with Fe^{3+} compresses the Ti-O bond distance henceforth intensifying the Ti-O bond interaction and reducing the cell size which is in accordance with the XRD results.

3.2. Room temperature Dielectric studies

Fig. 9(a) & (b) shows the room temperature (RT) variation of dielectric constant $\varepsilon'(\omega)$ and loss tangent ($\tan\delta$), respectively, of the prepared Fe-doped PZT ceramics for a wide frequency range (100 Hz – 1MHz), assembled in capacitor configuration. It is evident from Fig. 9(a) & (c) that the RT dielectric constant for all the frequencies decreased as soon as Fe-doping was introduced and kept on decreasing with further substitution which may be attributed to the creation of oxygen vacancies and secondary magneto-plumbite phase that interferes with the ferroelectric domain wall motion. The defect dipole complexes, Fe^{3+}–VO^{2-}–Fe^{3+}, associated with oxygen vacancies, having low stability of dipole direction, align themselves along the domain's polarization direction. Thus, they make the domain walls more stable and rigid towards any movement, causing the observed decrease in dielectric constant [2, 15, 19, 24, 38, 39, 43]. This decrease in the RT value of dielectric constant with increase in Fe-doping in PZT ceramics has also been reported in other literatures, Fig. 9(d). It may be observed that dielectric constant showed low frequency dielectric dispersion which seems to reduce with increase in frequency. The low frequency dielectric dispersion is reported to be caused by space-charge accumulation, while the space charge polarization of grain-grain boundary interface is mainly responsible for the dielectric dispersion at high frequencies.

In Fig. 9(b) & (c) the tangent loss ($\tan\delta$) of PZTF ceramic samples was found to increase with increase in Fe-doping at all frequencies. This was attributed to high Fe-concentrations along with increased oxygen vacancies leading to reduced resistivity of the ceramic samples. For Fe-doping concentrations of 0 and 5 at%, the loss decreased with increase in frequency. While for the rest of compositions, it started with a decrease up till 10^4 Hz, after which a peak was observed which may be attributed to the relaxation peak corresponding to the secondary phase introduced at higher doping concentrations.

3.3 Multiferroic Study

3.3.1. Ferroelectric Study

The variation of electric polarization at room temperature with applied electric field is shown in Fig. 10. The pure PZT ceramic sample (PZT-F0) showed saturation polarization (P_s) of 20 $\mu C/cm^2$ and remnant polarization (P_r) of 16 $\mu C/cm^2$, along with coercive field of 9 kV/cm. The polarization was observed to fall sharply after incorporation of 5 at% Fe-dopant (PZT-F5) into the PZT ceramic system and kept on decreasing with further doping, Fig. 11. A similar trend has been observed by others for lower concentrations of Fe-doping, inset of Fig. 11. The plots of Fig. 9 (b), (c), and (d) are cigar-shaped loops that are characteristic of lossy dielectrics which is typical of multiferroics such as $BiFeO_3$ dominated by high leakage currents. The larger leakage currents in magneto-electrics often result from mixed valence for the magnetic ions (eg. Fe^{2+} and Fe^{3+}), from oxygen vacancies, or from both [49]. Incorporation of Fe^{3+} ions creates defect dipole complexes associated with the charge compensating oxygen vacancies leading to the hardening effect and reduced ferroelectric properties. Thus, the P-E hysteresis loops for the Fe-doped PZT ceramics were lossy and unsaturated. Also, with decrease in grain size the grain boundary density increases which are non-ferroelectric in nature. Hence, a depolarizing field is created as

the surface polarization is reduced. This leads to reduced remnant polarization. The decreased grain size promotes formation of 90° domain walls leading to increase in repulsion between adjoining domain walls which obstructs their motion and re-orientation against the applied electric field. Also, the decreased grain size leads to reduced domain size. Effectively, all this results in reduced electric polarization and hard ferroelectric effects. The unsaturated PE loops results due to the clamping of the domain walls in smaller grains.

The electric polarization, which is the result of the BO_6 vibrations in the ABO_3 ferroelectric perovskite, is also affected by the change in the mean bond length between B cation and oxygen ion. A larger room for vibration at B-site is believed to result in larger polarization as when the electric field is applied the smaller B cation can wriggle effortlessly without disrupting the BO_6 octahedra. Thus, the polarization is reduced when bigger Fe^{3+} ions shrunk the available vibrational room by substituting the smaller Ti/Zr ions. Meanwhile the reduction in tetragonal distortion due to changes in lattice parameters also lead to the suppression of the ferroelectric properties [2, 15, 24, 39].

3.3.2. Ferromagnetic Study

It is an established fact that PZT is diamagnetic in nature; still, ferromagnetism can be established via introduction of impurities, defects, oxygen vacancies, and F-centers. Room temperature (RT) variation of magnetization (M) with applied magnetic field (H) PZT ceramics doped with Fe^{3+} ions are shown in Fig. 12(a). It can be observed that the undoped PZT ceramic (inset of Fig. 12(a)) shows a diamagnetic curve indicating its characteristic behavior. However, the introduction of Fe^{3+}-doping at 0.05 concentration in PZT ceramic transformed the M-H curve to S-type loop representing manifestation of ferromagnetic behavior and decrease in the diamagnetic contribution of PZT. Further increase in the content of Fe-doping lead to appearance of the conventional ferromagnetic hysteresis loops with increased magnetization, Fig. 12(b) &

Table 4. Thus the Fe^{3+}-doped PZT ceramics demonstrated ferromagnetic properties at RT (300K). Analogous observations of ferromagnetism at RT have been reported by Ren et al and by Verma et al in the case of PT nano-crystals and by Puthucheri et al in PZT (Fig. 12(c)) [50, 51, 15]. The observed ferromagnetic effect had been explained using the mechanism of F-center exchange in Fe^{3+}–VO^{2-}–Fe^{3+} assemblies [52]. F-center is an electron stuck within the oxygen vacancy occupying the orbital overlapping the d-shells of the adjacent two iron atoms. The coupling between the down-spin electron and up-spins of the two Fe^{3+} ions is known as the F-center exchange responsible for the ferromagnetism in the material. Since the bulk is being doped with Fe^{3+}, there is thus contribution of para-magnetism as the Fe^{3+} ions inherently possess paramagnetic characteristics. While some antiferromagnetic effect is also present due to super-exchange interaction within Fe^{3+}–O–Fe^{3+} groups. Thus, the ferromagnetism observed in Fe-doped PZT ceramics is the resultant effect of the competition between the paramagnetic, anti-ferromagnetic and ferromagnetic contributions of the Fe^{3+} ions, Fe^{3+}–O–Fe^{3+} and Fe^{3+}–VO^{2-}–Fe^{3+} groups, respectively. As per reported literature, the paramagnetic effect of Fe^{3+} ions dominate the other two effects at higher doping concentrations and thus leads to linearization of the M-H curves. However, in present work the M-H curves are saturated at higher Fe-doping concentrations. This may be attributed to the ferromagnetic effect of the secondary magneto-plumbite phase [20, 38] formed in our samples which along with the ferromagnetic coupling due to the F-center exchange lead to the observed saturated M-H curves.

4. Effects of doping-

The doping of PZT ceramics with Fe^{3+} ions can be witnessed in its structural, dielectric, ferro-electric and –magnetic properties. The substitution of the smaller Ti^{4+} ions by the larger Fe^{3+} ions

in the PZT ceramics lead to decrease in c/a ratio and crystallite size which can be confirmed from the XRD data analysis (Fig. 5(a) and Table 2). The Fe^{3+} substitution also caused decrease in grain size (Fig. 6 & 7 and Table 2) and it was attributed to the accumulation of immobile Fe^{3+} ions at the grain boundaries and to the formation of secondary magneto-plumbite phase. The dielectric constant at a particular frequency decreased with increase in the Fe-doping concentration (refer to Fig. 9(b)) due to the increased oxygen vacancies and related dipole defect complexes which are known to interfere with domain wall mobility. The Fe-doping of PZT ceramic samples decreased their ferroelectric polarization, while the magnetization increased, Fig. 11 & 12(c). The unsaturated and lossy behavior of the ferroelectric loops was attributed to the increased oxygen vacancies and the associated defect dipole complexes. The decreased polarization was attributed to clamping of the domain walls in small sized grains, reduced tetragonality and larger size of Fe^{3+} ions. The increased magnetization at lower doping concentrations was due to the dominant ferromagnetic effect of the F-center exchange mechanism, while the secondary magneto-plumbite phase generated at higher doping concentrations was responsible for the observed saturated ferromagnetic loops.

5. Conclusion

In summary, the effect of Fe^{3+}-doping in the PZT ceramics prepared via conventional solid-state reaction method at higher doping concentrations, i.e. at Fe = 0, 5, 10, 15 and 20 at%, has been investigated in this work. The prepared PZTF ceramic samples were studied for their structural, dielectric and multi-ferroic properties using XRD, SEM, Raman scattering, dielectric capacitive, P-E and B-H hysteresis measurements. The XRD spectra exhibited a complete tetragonal phase for PZTF ceramics and a decreasing trend was observed in c/a ratio and crystallite size with increase in Fe^{3+} dopant concentration. Similar decreasing trend was observed for the grain size.

The Raman spectra in accordance with the XRD results confirmed a decrease in unit cell size. The dielectric constant for a particular frequency was observed to decrease with increase in the Fe-doping concentration. The higher Fe^{3+}-doping concentration led to decreased ferroelectric polarization while the magnetization increased due to generation of secondary magneto-plumbite phase along with F-center exchange mechanism.

Acknowledgments

The authors are thankful to the DST, Ministry of Science and Technology, Govt. of India for financial assistance. One of the authors (A.S.) would like to thank the DST, Ministry of Science and Technology, Govt. of India for award of Young Scientist and BOYSCAST Fellowship executed in USA and also thankful to Professor R. S. Katiyar, UPR, DOE, and NASA (USA) for lab facility made available at University of Puerto Rico, USA during BOYSCAST Fellowship.

References

[1] A.K.S. Chauhan, V. Gupta, K. Sreenivas, Dielectric and piezoelectric properties of sol-gel derived Ca doped $PbTiO_3$, Mater. Sci. Eng. B. 130 (2006) 81–88.

[2] D. Damjanovic, Ferroelectric, dielectric and piezoelectric properties of ferroelectric thin films and ceramics, Reports Prog. Phys. 61 (1998) 1267–1324.

[3] R. Jain, A.K.S. Chauhan, V. Gupta, K. Sreenivas, Piezoelectric properties of nonstoichiometric $Sr_{1-x}Bi_{2+2x/3}Ta_2O_9$ ceramics, J. Appl. Phys. 97, 12 (2005) 124101(1-6).

[4] N. Setter, D. Damjanovic, L. Eng, G. Fox, S. Gevorgian, S. Hong, A. Kingon, H. Kohlstedt, N.Y. Park, G.B. Stephenson, I. Stolitchnov, A.K. Taganstev, D. V. Taylor, T. Yamada, S. Streiffer, Ferroelectric thin films: Review of materials, properties, and applications, J. Appl. Phys. 100, 5 (2006) 051606 (1-46).

[5] K. Sharma, A. Singh, Advances in Photovoltaic Behavior of Ferroelectric $BiFeO_3$, J.

Nanosc. Tech. 2, 2 (2016) 85–90.

[6] B. Jaffe, W. R. Cook Jr., H. Jaffe, Piezoelectric Ceramics, Academic Press Inc. 1971.

[7] N. Izyumskaya, Y.I. Alivov, S.J. Cho, H. Morkoç, H. Lee, Y.S. Kang, Processing, structure, properties, and applications of PZT thin films, Crit. Rev. Solid State Mater. Sci. 32 (2007) 111–202.

[8] A. Presas, Y. Luo, Z. Wang, D. Valentin, M. Egusquiza, A Review of PZT Patches Applications in Submerged Systems, Sensors. 18 (2018) 1–21.

[9] L.W. Martin, A.M. Rappe, Thin-film ferroelectric materials and their applications, Nat. Rev. Mater. 2 (2016) 1–14.

[10] R.E. Newnham, G.R. Ruschau, Smart Electroceramics, J. Am. Ceram. Soc. 74 (1991) 463–80.

[11] J.F. Scott, C.A.P. De Araujo, Ferroelectric Memories, Science. 246, 4936 (1989) 1400–1405.

[12] J.F. Scott, Applications of Modern Ferroelectrics, Science. 315, 5814 (2007) 954–959.

[13] S.Y. Yang, J. Seidel, S.J. Byrnes, P. Shafer, C.H. Yang, M.D. Rossell, P. Yu, Y.H. Chu, J.F. Scott, J.W. Ager, L.W. Martin, R. Ramesh, Above-bandgap voltages from ferroelectric photovoltaic devices, Nat. Nanotechnol. 5 (2010) 143–147.

[14] G. Haertling, Ferroelectric ceramics: history and technology, J. Am. Ceram. Soc. 82 (1999) 718–818.

[15] S. Puthucheri, P.K. Pandey, N.S. Gajbhiye, A. Gupta, A. Singh, R. Chatterjee, S.K. Date, Microstructural, Electrical, and Magnetic Properties of Acceptor-Doped Nanostructured Lead Zirconate Titanate, J. Am. Ceram. Soc. 94 (2011) 3941–3947.

[16] A. Banerjee, A. Bandyopadhyay, S. Bose, Influence of La_2O_3, SrO, and ZnO addition on PZT, J. Am. Ceram. Soc. 89 (2006) 1594–1600.

[17] B.W. Lee, E.J. Lee, Effects of complex doping on microstructural and electrical properties of PZT ceramics, J. Electroceramics. 17 (2006) 597–602.

[18] K. Ramam, M. Lopez, Effect of acceptor and donor dopants on ferroelectric and piezoelectric properties of lead zirconate titanate ceramics, Phys. Status Solidi. 203 (2006) 3852–3860.

[19] S.B. Majumder, B. Roy, R.S. Katiyar, S.B. Krupanidhi, Effect of neodymium (Nd) doping on the dielectric and ferroelectric characteristics of sol-gel derived lead zirconate titanate (53/47) thin films, J. Appl. Phys. 90 (2001) 2975–2984.

[20] H. Kleebe, S. Lauterbach, L. Silvestroni, H. Kungl, M.J. Hoffmann, E. Erdem, R. Eichel, Formation of magnetic grains in ferroelectric $Pb(Zr_{0.6}Ti_{0.4})O_3$ ceramics doped with Fe^{3+} above the solubility limit, Appl. Phys. Lett. 94 (2009) 142901(1–3).

[21] E. Erdem, R. Eichel, C. Fetzer, I. Dézsi, S. Lauterbach, H. Kleebe, A.G. Balogh, Site of incorporation and solubility for Fe ions in acceptor-doped PZT ceramics, J. Appl. Phys. 107 (2010) 054109(1-5).

[22] R.A. Eichel, H. Mestric, K.P. Dinse, A. Ozarowski, J. Van Tol, L.C. Brunel, H. Kungl, M.J. Hoffmann, High-field / high-frequency EPR of paramagnetic functional centers in Cu^{2+} - and Fe^{3+} -modified polycrystalline $Pb[Zr_xTi_{1-x}]O_3$ ferroelectrics, Magn. Reson. Chem. 43 (2005) 166–173.

[23] R. Eichel, Defect structure of oxide ferroelectrics-valence state, site of incorporation, mechanisms of charge compensation and internal bias fields, J . Electroceram. 19 (2007) 9–21.

[24] S. Samanta, V.S.K. Sethupathi, Effect of Nb and Fe co-doping on microstructure , dielectric response , ferroelectricity and energy storage density of PLZT, J. Mater. Sci. Mater. Electron. 29 (2018) 20383–20394.

[25] A. Singh, Z. Raza, P.M. Vilarinho, V. Gupta, R.S. Katiyar, Influence of thickness on optical and structural properties of $BiFeO_3$ thin films : PLD grown, Mater. Res. Bull. 49 (2014) 531–536.

[26] K. Mori, M. Wuttig, Magnetoelectric coupling in Terfenol-D / polyvinylidenedifluoride composites, Appl. Phys. Lett. 81 (2002) 100–101.

[27] J. Wang, J.B. Neaton, H. Zheng, V. Nagarajan, S.B. Ogale, B. Liu, D. Viehland, V. Vaithyanathan, D.G. Schlom, U. V Waghmare, N.A. Spaldin, K.M. Rabe, M. Wuttig, R. Ramesh, Epitaxial $BiFeO_3$ Multiferroic Thin Film Heterostructures, Science. 299 (2003) 1719–1722.

[28] L.W. Martin, R. Ramesh, Multiferroic and magnetoelectric heterostructures, Acta Mater. 60 (2012) 2449–2470.

[29] K. Sharma, A. Singh, Progress in the Growth and Characterization of Nano-Structured Bismuth Ferrite Thin Films, J. Adv. Chem. Sci. 2 (2016) 241–245.

[30] J.F. Scott, Data Storage: Multiferroic memories, Nat. Mater. 6 (2007) 256–257.

[31] L.W. Martin, Y.H. Chu, R. Ramesh, Advances in the growth and characterization of magnetic, ferroelectric, and multiferroic oxide thin films, Mater. Sci. Eng. R. 68 (2010) 89–133.

[32] P. Gonnard, M. Troccaz, Dopant distribution between A and B Sites in the PZT Ceramics of Type ABO_3, J. Solid State Chem. 23 (1978) 321–326.

[33] N. Kumari, S. Monga, M. Arif, N. Sharma, A. Singh, V. Gupta, P.M. Vilarinho, K. Sreenivas, R.S. Katiyar, Higher permittivity of Ni-doped lead zirconate titanate, $Pb[(Zr_{0.52}Ti_{0.48})_{(1-x)}Ni_x]O_3$, ceramics, Ceram. Int. (2018), in press.

[34] Y. Kawamura, N. Matsumoto, H. Kamataki, K. Mukae, Microstructure and Piezoelectric Properties of PZT Based Ceramics, Jpn. J. Appl. Phys. 28 (1989) 77–79.

[35] L. Hankey, J. V Biggers, Solid-state Reactions in the System PbO-TiO_2-ZrO_2, J. Am. Ceram. Soc. 64 (1981) C172–C173.

[36] M. Hammer, M.J. Hoffmann, Sintering model for mixed-oxide-derived lead zirconate titanate ceramics, J. Am. Ceram. Soc. 81 (1998) 3277–3284.

[37] L. Silvestroni, H. Kleebe, H. Kungl, S. Lauterbach, M. Mu, M.J. Hoffmann, Lead Zirconate Titanate – Magnetoplumbite Composites : A First Step Towards Multiferroic Ceramics, 92 (2009) 2362–2367.

[38] G.H. Khorrami, A.K. Zak, S.M. Banihashemian, Magnetic and dielectric properties on sol-gel combustion synthesis of $Pb(Zr_{0.52},Ti_{0.43}X_{0.05})O_3$ (X = Fe, Ni, and Co) nanoparticles, Adv. Powder Technol. 25 (2014) 1319–1324.

[39] E.V. Ramana, F. Figueiras, A. Mahajan, D.M. Tobaldi, B.F.O. Costa, M.P.F. Graça, M.A. Valente, Effect of Fe-doping on the structure and magnetoelectric properties of $(Ba_{0.85}Ca_{0.15})(Ti_{0.9}Zr_{0.1})O_3$ synthesized by a chemical route, J. Mater. Chem. C. 4 (2016) 1066–1079.

[40] A. Singh, V. Gupta, K. Sreenivas, R.S. Katiyar, Influence of Ca additives on the optical and dielectric studies of sol – gel derived $PbTiO_3$ ceramics, J. Phys. Chem. Sol. 68 (2007) 119–123.

[41] Z.R. Khan, M. Arif, A. Singh, Development and study of the structural and optical properties of hexagonal ZnO nanocrystals, Int. Nano Lett. 2 (2012) 1–5.

[42] A.K.S. Chauhan, K. Sreenivas, TG-DTA and FT-IR Studies on Sol-Gel Derived $Pb_{(1-x)}Ca_xTiO_3$, Ferroelectrics. 324 (2005) 77–81.

[43] T.B. Weston, A.H. Webster, V.M. Mcnamara, Lead Zirconate- Lead Titanate Piezoelectric Ceramics with Iron Oxide Additions, J. Am. Ceram. Soc. 52 (1969) 253–257.

[44] J. Frantti, V. Lantto, Structural studies of Nd-modified lead zirconate titanate ceramics between 11 and 680 K at the morphotropic phase boundary, Phys. Rev. B. 56 (1997) 221–236.

[45] J. Rouquette, J. Haines, V. Bornand, M. Pintard, P. Papet, J.L. Sauvajol, Use of resonance Raman spectroscopy to study the phase diagram of $PbZr_{0.52}Ti_{0.48}O_3$, Phys. Rev. B. 73 (2006) 224118(1-5).

[46] K.C. V. Lima, A.G.S. Filho, A.P. Ayala, J.M. Filho, P.T.C. Freire, F.E.A. Melo, E.B. Araújo, J.A. Eiras, Raman study of morphotropic phase boundary in $PbZr_{1-x}Ti_xO_3$ at low temperatures, Phys. Rev. B. 63 (2001) 184105(1-5).

[47] E. Buixaderas, I. Gregora, M. Savinov, J. Hlinka, L. Jin, Compositional behavior of Raman-active phonons in $Pb(Zr_{(1-x)}Ti_x)O_3$ ceramics, Phys. Rev. B. 91 (2015) 14104(1–9).

[48] A. Singh, K. Sreenivas, R.S. Katiyar, V. Gupta, Evidence of pseudocubic structure in sol-gel derived $Pb_{(1-x)}Ca_xTiO_3$ (x = 0.35 – 0.48) ceramic by dielectric and Raman spectroscopy, J. Appl. Phys. 102 (2007) 74110(1-8).

[49] J.F. Scott, Ferroelectrics go bananas, J. Phys.: Condens. Matter. 20 (2008) 021001(1-2).

[50] Z. Ren, G. Xu, X. Wei, Y. Liu, X. Hou, P. Du, W. Weng, G. Shen, G. Han, Room-temperature ferromagnetism in Fe-doped $PbTiO_3$ nanocrystals, Appl. Phys. Lett. 91 (2007) 63106(1-3).

[51] K.C. Verma, R.K. Kotnala, N.S. Negi, Improved dielectric and ferromagnetic properties in Fe-doped $PbTiO_3$ nanoparticles at room temperature, Appl. Phys. Lett. 92 (2008) 152902(1–3).

[52] J.M.D. Coey, A.P. Douvalis, C.B. Fitzgerald, M. Venkatesan, Ferromagnetism in Fe-doped SnO_2 thin films, Appl. Phys. Lttr. 84, 8 (2004) 1332-34.

[53] J. Suchanicz, N.-T.H. Kim-Ngan, K. Konieczny, I. Jankowska-Sumara, D. Sitka, D. Goc-

Jaglo, and A.G. Balogh, Influence of combined external stress and electric field on electric properties of 0.5% Fe-doped lead zirconate titanate ceramics, J. Appl. Phys. 106 (2009) 094109(1-4).

[54] L. Jin, Z. He, and D. Damjanovic, Nanodomains in Fe^{+3}-doped lead zirconate titanate ceramics at the morphotropic phase boundary do not correlate with high properties, Appl. Phys. Lett. 95 (2009) 012905(1-3).

[55] B. P. Kumar, S.R. Sangawar, and H.H. Kumar, Structural and electrical properties of double doped (Fe^{3+} and Ba^{2+}) PZT electroceramics, Ceram. Int. 40, 2 (2014) 3809-3812.

Figure Captions

Fig. 1 Perovskite structure of PZT.

Fig. 2 Flow Chart for preparation of Fe-doped PZT by solid state reaction method.

Fig. 3 XRD patterns for Fe-doped PZT ceramics.

Fig. 4 (a) Lattice constant and tetragonality factor variation with Fe-Concentration.

(b) XRD peaks in the range 42-47° for PZTF ceramic samples.

(c) Variation of strain with Fe-Concentration for PZTF ceramic samples.

Fig. 5 (a) Variation of crystallite size of PZTF ceramic samples with change in Fe-concentration; Inset shows the crystallite size values reported by other workers.

(b) Variation of cell volume of PZTF ceramic samples with change in Fe-concentration.

Fig. 6 SEM images of (a) PZT-F0, (b) PZT-F5, (c) PZT-F10, (d) PZT-F15, and (e) PZT-F20 ceramic samples.

Fig. 7 Variation of grain size of PZTF ceramic samples with change in Fe-concentration; Inset shows the grain size values reported by other workers.

Fig. 8 (a) Raman spectra of PZTF ceramics samples.

(b) Raman mode frequencies as a function of Fe-Concentration for PZTF ceramic samples.

Fig. 9 (a) Room temperature frequency variation of dielectric constant of PZTF ceramic samples.

(b) Room temperature frequency variation of dielectric loss of PZTF ceramic samples.

(c) Variation of Room temperature Dielectric Constant and loss for PZTF ceramic samples measured at 1 and 10 kHz.

(d) Variation of dielectric constant of PZTF ceramic samples with change in Fe-concentration. Inset shows the values of dielectric constant reported by other workers.

Fig. 10 P-E hysteresis curves for (a) PZT-F0, (b) PZT-F5, (c) PZT-F10, (d) PZT-F15, and (e) PZT-F20 ceramic samples.

Fig. 11 Variation of remnant polarization of PZTF ceramic samples with change in Fe-concentration. Inset shows the values of remnant polarization reported by other workers.

Fig. 12 (a) B-H hysteresis curves for PZTF ceramic samples.

(b) Saturation magnetization, remnant magnetization and coercive magnetic field as a function of Fe-Concentration for PZTF ceramic samples.

(c) Variation of saturation magnetization of PZTF ceramic samples with change in Fe-concentration. Inset shows the values of saturation magnetization reported by other workers.

Table Caption

Table 1 Properties of Fe-doped PZT at different doping concentrations reported in literature and in the present work.

Table 2 The lattice parameters, tetragonality factor, strain, crystallite size, cell size and grain size of the pure and Fe doped PZTs.

Table 3 Raman Modes in PZTF ceramic samples.

Table 4 Saturation magnetization, remnant magnetization and coercive magnetic field value for PZTF ceramic samples

Behavior of multifunctional acceptor-doped PZT ceramics: Cation substitution at higher doping concentration

Nitu Kumari,[1,2] Shagun Monga,[1] Mohd. Arif,[1] Neeraj Sharma,[1] Amit Sanger,[3] Arun Singh,[1,6*] Paula. M. Vilarinho,[4] Vinay Gupta,[5] K. Sreenivas,[5] Ram S. Katiyar,[6] James F. Scott[7]

[1]*Advanced Electronic and Nano-Materials Laboratory, Department of Physics, Jamia Millia Islamia University, New Delhi- 110025, India*
[2]*Department of Physics, TMB University, Bhagalpur, 812007 India*
[3]*Department of Materials Science and Engineering, Ulsan National Institute of Science and Technology, Ulsan 44919, Republic of Korea*
[4]*Department of Ceramics and Glass Engineering, University of Aveiro, 3810-193 Aveiro, Portugal*
[5]*Electronic Materials and Device Laboratory, Department of Physics and Astrophysics, University of Delhi, Delhi-110 007, India*
[6]*SPECLAB, Department of Physics, University of Puerto Rico, San Juan 00931, Puerto Rico, USA.*
[7]*Department of Physics, University of St Andrews, St Andrews-KY16 9SS, UK*

a) ***Corresponding author***
Dr. Arun Singh,
Assistant Professor
Department of Physics, Faculty of Natural Science
Jamia Millia Islamia (a Central University),
New Delhi, India, 110025
Email:***arunsingh07@gmail.com,***
Tel.: +91-26984631; +91-9891223302

Table. 1 Properties of Fe-doped PZT at different doping concentrations reported in literature and in the present work.

Fe-Concentration (at%)	Crystallite Size (nm)	Grain Size (µm)	Dielectric Constant at 1 kHz	Remnant Polarization (µC/cm^2)	Saturation Magnetization (emu/gm)	Ref.
0	12	-	~588	10	-	Puthucheri et al, [15]
	-	5.4	~1410	-	-	Weston et al, [43]
	23	2.5	512	-	-	Khorrami et al, [38]
	-	8	-	10	-	Jin et al, [54]
	23.27	0.41	722	16	-	Present work
0.001	-	-	1160	-	-	Weston et al, [43]
0.002	-	2.7	971	-	-	Weston et al, [43]
0.004	-	2.7	796	-	-	Weston et al, [43]
0.005	-	2	~2500	5.35	-	Suchanicz et al, [53]
0.006	-	3	664	-	-	Weston et al, [43]
0.008	-	2.9	596	-	-	Weston et al, [43]
0.01	-	2	~960	-	-	Kumar et al, [55]
	-	2	-	~5.5	-	Jin et al, [54]
0.012	-	3.1	484	-	-	Weston et al, [43]
0.02	15	-	~760	15	0.011	Puthucheri et al, [15]
0.04	12	-	~760	~10	0.02	Puthucheri et al, [15]
0.05	16	-	418	-	8000	Khorrami et al, [38]
	13.31	0.25	619	6	0.20	Present work
0.06	8	-	~580	2.5	0.03	Puthucheri et al, [15]
0.10	13.87	0.21	485	0.55	1.1	Present work
0.15	15.75	0.17	351	0.42	1.7	Present work
0.20	16.50	0.15	327	-	2.5	Present work

Table 2: The lattice parameters, tetragonality factor, strain, crystallite size, cell size and grain size of the pure and Fe-doped PZTs.

Sample	Structure	Lattice parameter (nm)	c/a	Crystallite size (D) Scherrer (nm)	Strain (ε) x 10^{-2}	Cell Size (nm^3)	Grain Size (μm) SEM
PZT	Tetragonal	a = b = 0.4018, c = 0.4139	1.030	23.27	0.0041	0.0668	0.41
Fe (0.05) - PZT	Tetragonal	a = b = 0.4006, c = 0.4095	1.022	13.31	0.0074	0.0657	0.25
Fe (0.10) - PZT	Tetragonal	a = b = 0.4020, c = 0.4095	1.019	13.87	0.0069	0.0662	0.21
Fe (0.15) - PZT	Tetragonal	a = b = 0.4019, c = 0.4113	1.023	15.75	0.0062	0.0664	0.17
Fe (0.20) - PZT	Tetragonal	a = b = 0.4020, c = 0.4110	1.022	16.50	0.0058	0.0664	0.15

Table. 3. Raman Modes in PZT-Fe ceramic samples

Material ↓	Raman Modes (cm^{-1})							
	E(1TO)	**E(1LO)**	**A_1(1TO)**	**E(2TO)**	**E + B_1**	**A_1(2TO)**	**E(3TO)**	**E(3LO)**
PZT-Fe0	70.90	91.47	125.18	200.72	263.82	309.06	545.43	702.28
PZT-Fe5	71.70	92.91	125.18	199.28	263.82	321.08	553.73	705.17
PZT-Fe10	74.77	94.35	123.74	198.02	265.26	325.48	555.17	707.87
PZT-Fe15	75.63	92.29	135.20	201.81	270.10	338.30	558.97	709.91
PZT-Fe20	73.50	94.35	126.44	206.17	265.80	318.45	573.64	710.76

Table. 4. Saturation magnetization, remnant magnetization and coercive magnetic field value for PZTF ceramic samples.

Sample	Saturation Magnetization, emu/gm	Remnant Magnetization, emu/gm	Coercive Magnetic Field, kOe
PZT-F0	-	-	-
PZT-F5	0.20374	0.1413	1.752
PZT-F10	1.1013	0.70325	1.679
PZT-F15	1.7413	0.83593	1.642
PZT-F20	2.5218	1.7413	2.046

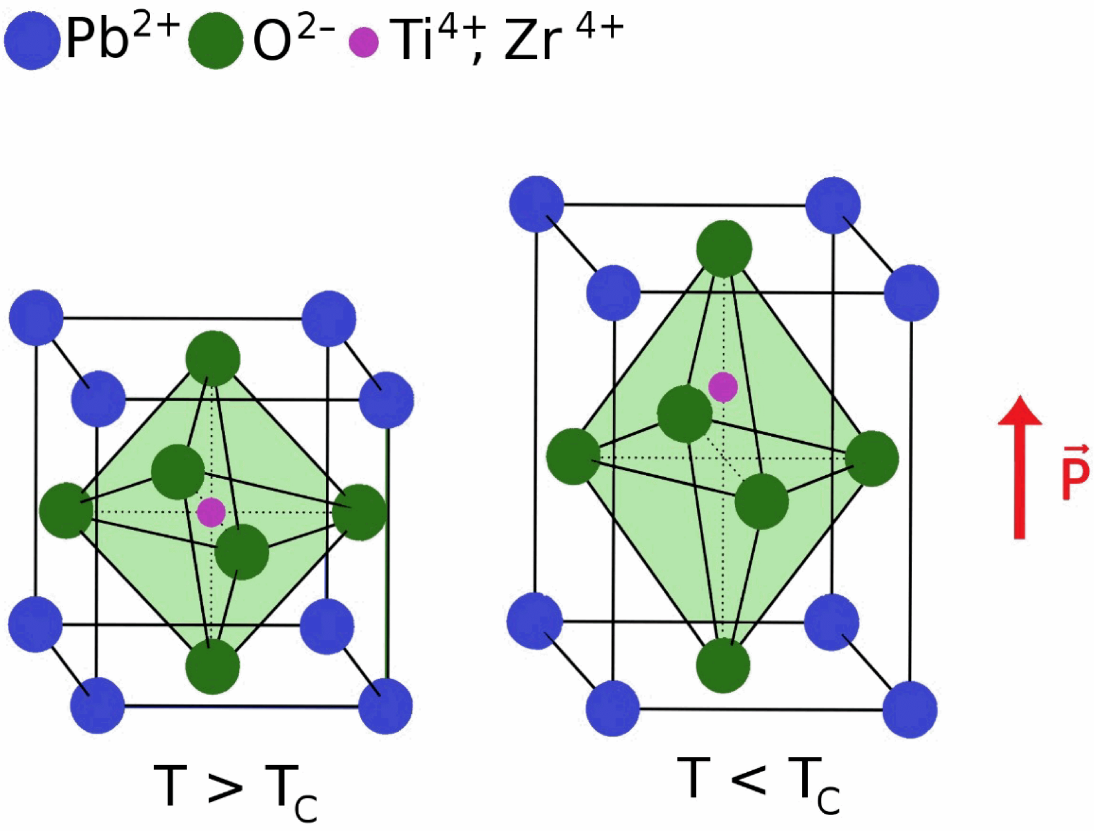

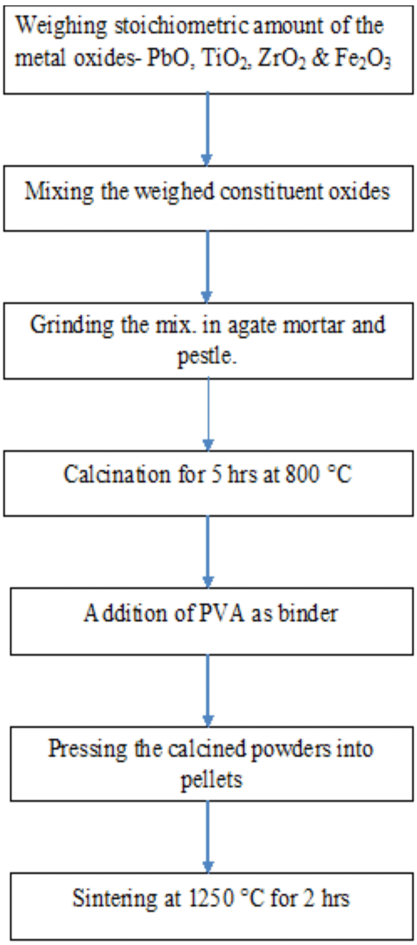

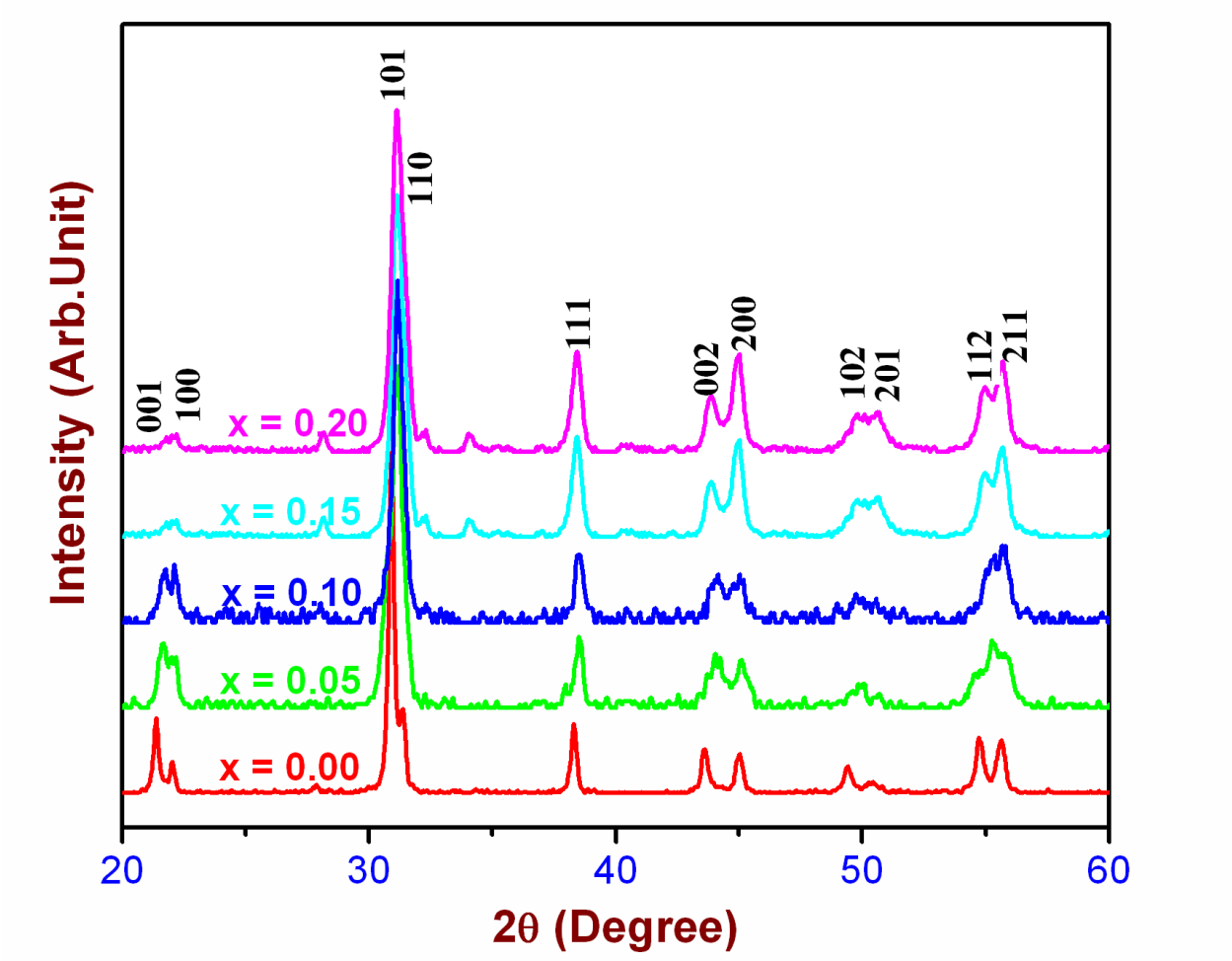

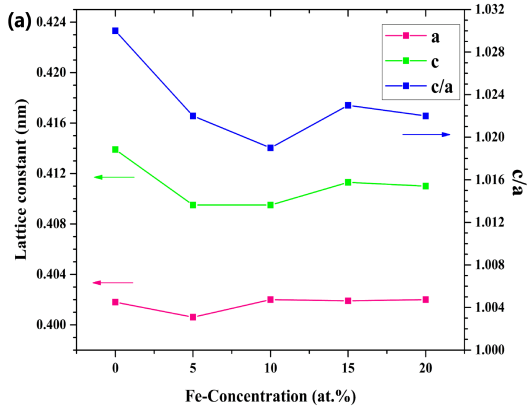

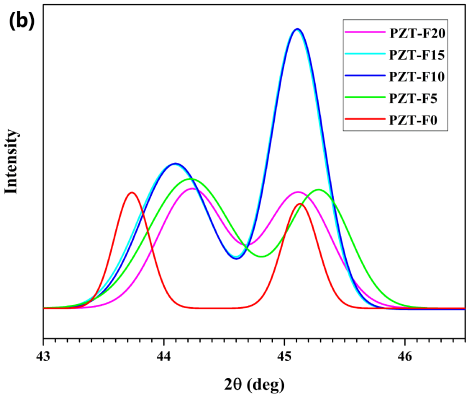

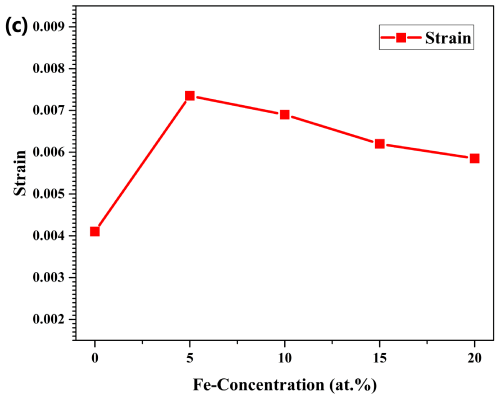

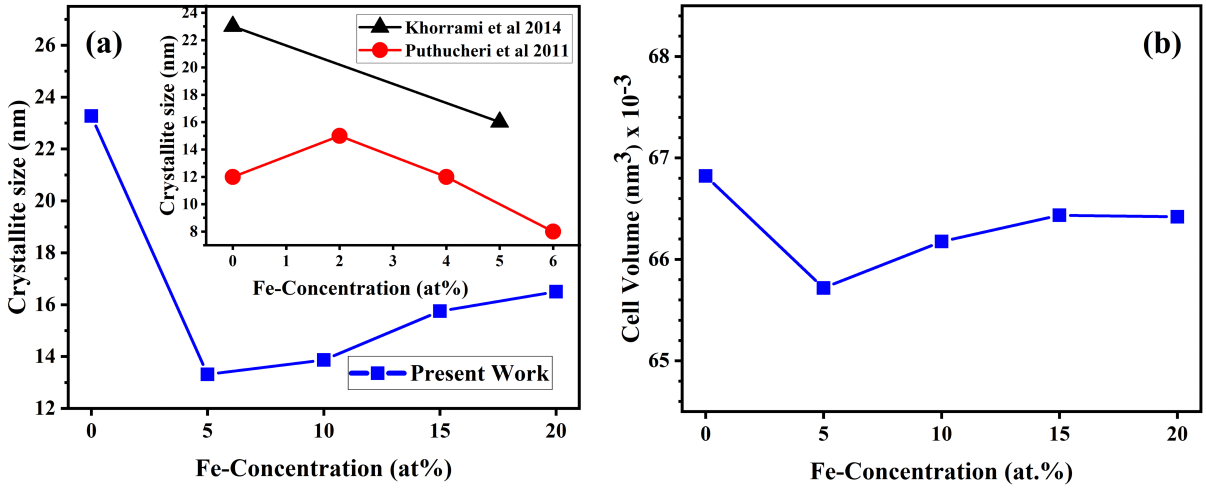

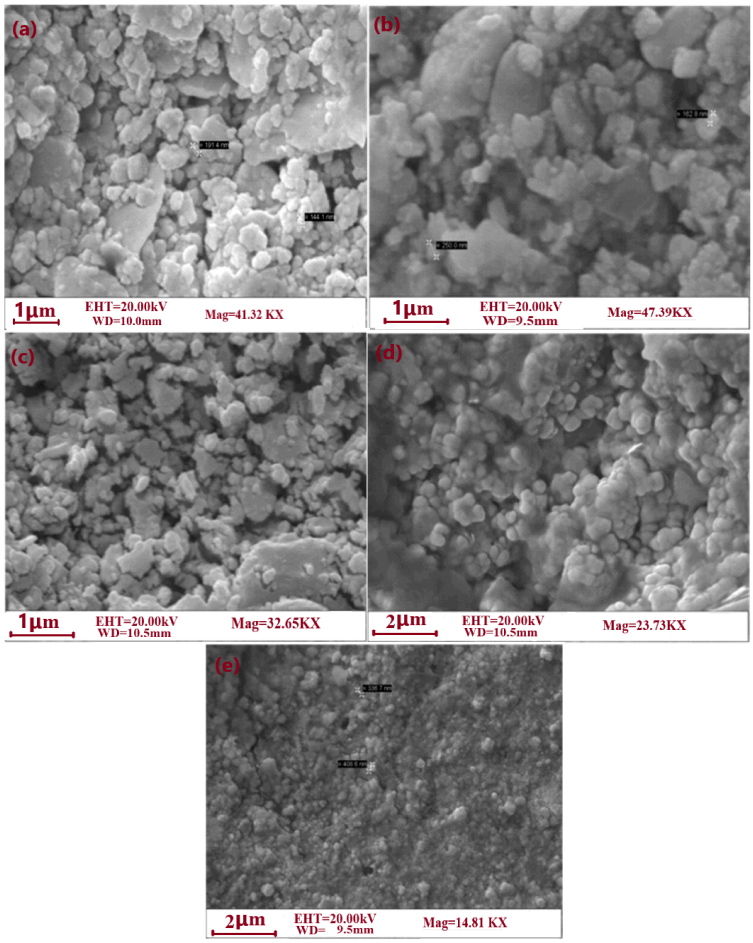

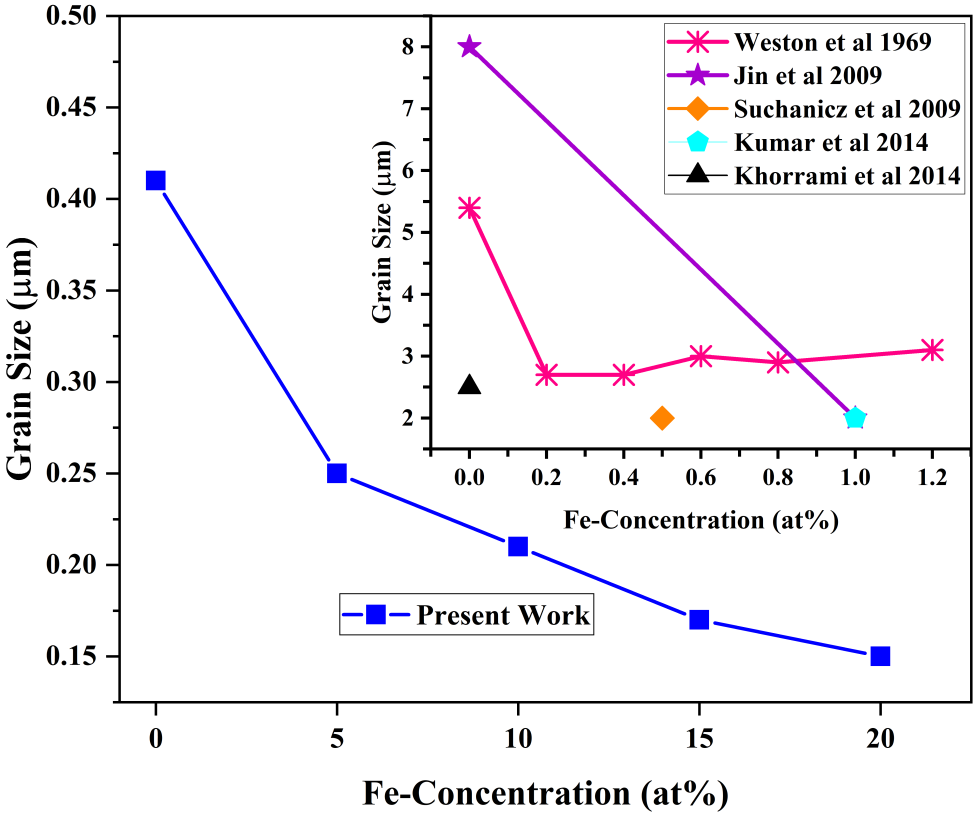

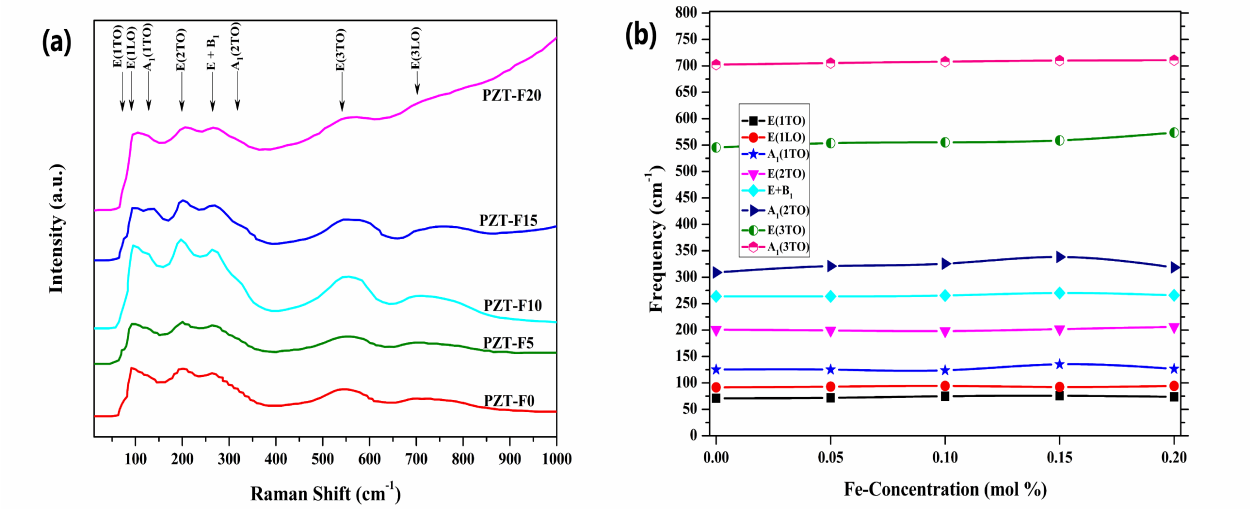

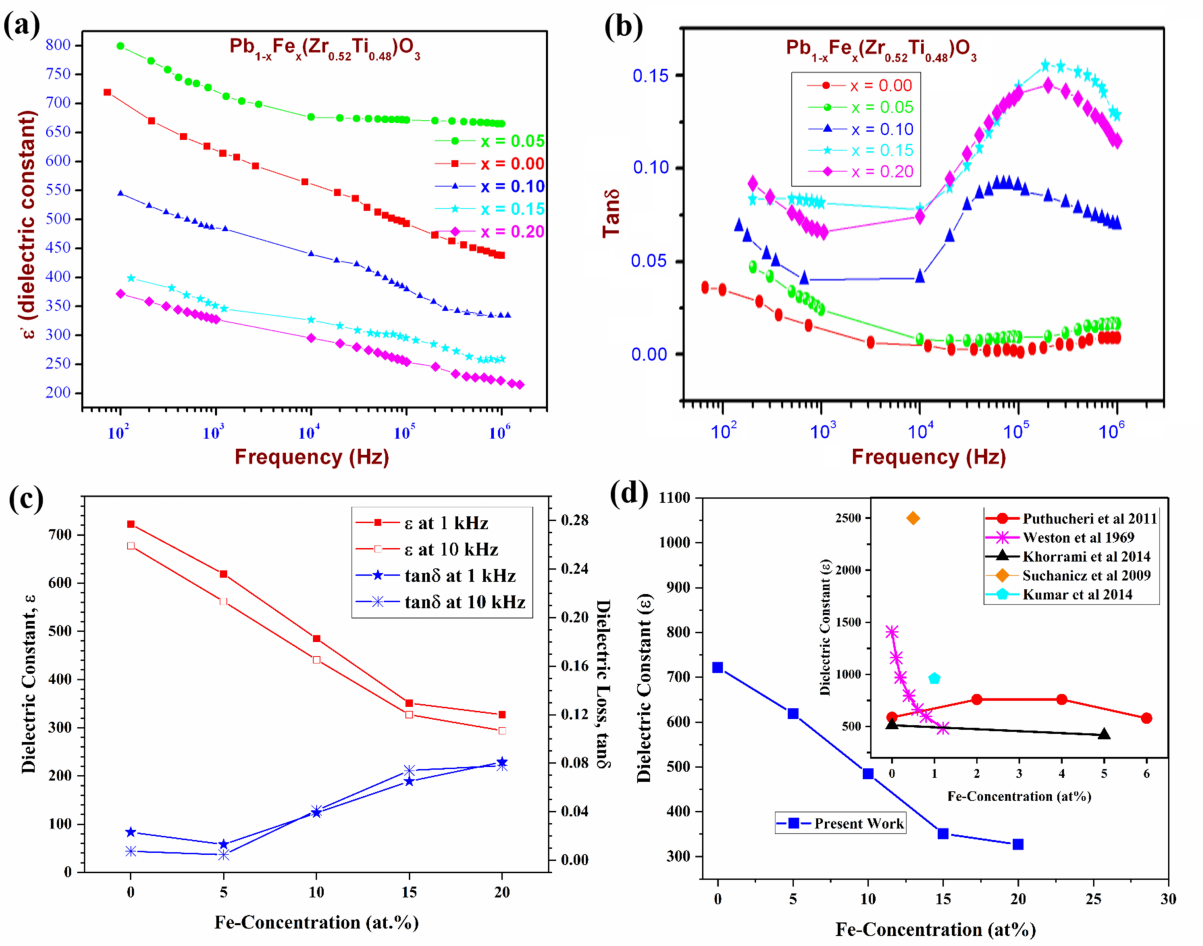

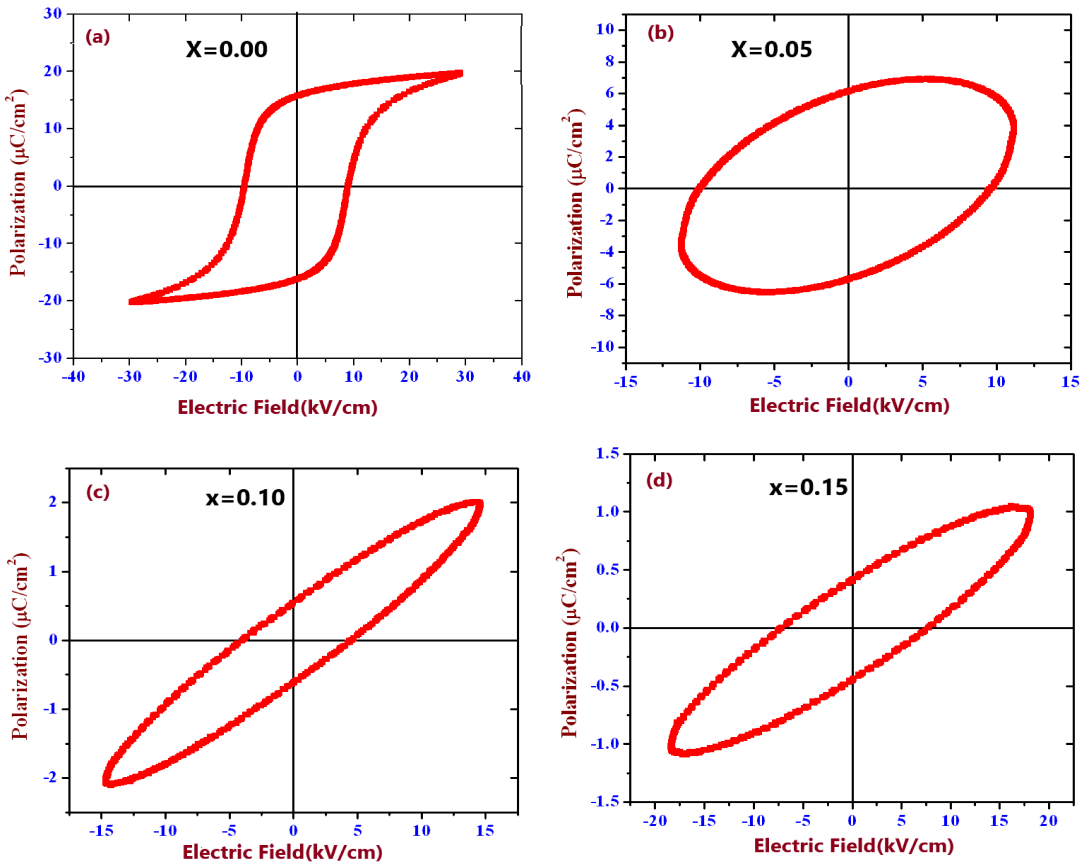
(a)
X=0.00
Polarization (μC/cm²)
Electric Field(kV/cm)
(b)
X=0.05
Polarization (μC/cm²)
Electric Field(kV/cm)
(c)
x=0.10
Polarization (μC/cm²)
Electric Field(kV/cm)
(d)
x=0.15
Polarization (μC/cm²)
Electric Field(kV/cm)